PERGAMON

Continental Shelf Research 19 (1999) 57–78

CONTINENTAL SHELF RESEARCH

Dispersion of produced water in a coastal environment and its biological implications

Libe Washburn[a,*], Shannon Stone[b], Sally MacIntyre[c]

[a]Institute for Computational Earth System Science, Department of Geography, University of California, Santa Barbara, CA 93106-3060, USA

[b]Bermuda Biological Station for Research, 17 Biological Lane, Ferry Reach, Bermuda, GE01, USA

[c]Marine Science Institute, University of California, Santa Barbara, CA 93106, USA

Received 20 October 1997; accepted 4 May 1998

Abstract

Produced water, a pollutant associated with offshore oil production, has been shown to have adverse effects on marine organisms. We conducted a study of the dispersion of a produced water plume from an outfall in the Santa Barbara Channel near Carpinteria, CA. Biological effects were studied previously in a series of experiments which examined the toxicity of ocean waters near the outfall. To define the changing ocean conditions around the outfall, we obtained time series observations of currents and water properties from July, 1992 to January, 1994. Near-field dispersion of the produced water is simulated with a buoyant plume model. Measured currents and density profiles are used as model inputs. Far-field dispersion is simulated with the current statistics combined with an elementary solution to the diffusion equation. The modeled depth of the plume varies strongly with season due to changing stratification. In spring and summer, the modeled plume is trapped below the surface. In fall and winter it extends over most of the water column and occasionally surfaces. Minimum initial dilution is ~ 100 in summer and ~ 500 in winter. Far-field modeling indicates along-isobath symmetry in produced water dispersion in the mid water column. This pattern agrees with the distribution of toxic effects from the biological studies. At 1000 m from the outfall, the farthest test sites in the biological studies, minimum dilutions range from 4000 to 4×10^5 when the plume is present. These estimates exceed the threshold for sub-lethal effects found by Krause (1993) in a sea urchin fertilization bioassay. Time averaged dilutions in the far-field are larger by factors of 10^2 to 10^3. © 1998 Elsevier Science Ltd. All rights reserved.

*Corresponding author. washburn@icess.ucsb.edu.

PII: S0278–4343(98)00068-5

1. Introduction

Produced water, one of the most important sources of pollution associated with oil production (Stephanson, 1992), is the water extracted along with oil in the drilling process. Large volumes of produced water are often generated because many oil deposits reside in or around groundwater aquifers. Produced water contains many contaminants including hydrocarbons, heavy metals, and chemical additives such as corrosion inhibitors to prevent damage to refinery equipment (Higashi et al., 1992).

Following its separation from oil, produced water is often discharged directly into the marine environment through submarine outfalls. The outfalls usually consist of a central pipe and a diffuser; the latter constructed with tee-risers and ports through which produced water is discharged. The tee-risers discharge the produced water horizontally in opposite directions. After discharge, produced water rises as a buoyant plume and mixes vigorously with ambient seawater. When ambient ocean waters are sufficiently stratified, the produced water rises to an equilibrium depth range where it spreads horizontally due to advection and mixing processes. When ambient waters are weakly stratified or well mixed, produced water rises to the top of the water column and forms a surface plume. The diffusers are designed to maximize initial dilution (Fischer et al., 1979). Until recently it was believed that the most significant biological impacts of produced water resulted from solids released with the discharge. These quickly settle out of the buoyant produced water plume and were thought to limit the spatial impact of solid components in the produced water.

Recent studies show broad spatial impacts in the marine environment due to the dissolved components of produced water. In a series of experiments described by Raimondi and Schmitt (1992), Osenberg et al. (1992), Krause (1993), and Krause et al. (1992) various invertebrate species were exposed to produced water discharged from a diffuser near Carpinteria, CA. Raimondi and Schmitt (1992) exposed larvae of red abalone (*Haliotis rufescens*) to produced water by attaching containers of them to moorings at 5, 10, 50, 100, 500, and 1000 m west of the diffuser and 5 and 1000 m east of the diffuser. They showed that survivorship of pre-competent larvae (those developmentally incapable of settling) was inversely correlated with distance from the diffuser, both east and west. Settlement, the ability to metamorphose, and viability were also inversely correlated with distance when pre-competent larvae were exposed. These effects extended to 100–500 m along isobaths away from the diffuser.

In another study at the Carpinteria site, Osenberg et al. (1992) found a decrease in growth rates along with a decline in the general condition and tissue production of mussels (*Mytilus californianus* and *M. edulis*) at up to 1000 m from the diffuser. Patterns of sub-lethal effects were inversely correlated with distance from the diffuser and were roughly symmetric to the east and west. Densities of some benthic organisms (e.g. nematodes) increased within 100 m of the diffuser while others (e.g. polychaetes) decreased. The changes in infaunal density were also symmetric east and west of the diffuser. Osenberg et al. (1992) suggest that settling of larger particles in the produced water or changes in sediment composition could account for the changes in infaunal density near the diffuser.

In laboratory experiments, adult purple sea urchins (*Strongylocentrotus purpuratus*) were exposed to varying concentrations of produced water from the Carpinteria diffuser. The experiments showed that the ability of purple sea urchin sperm to fertilize eggs was reduced for dilutions as high as 1,000,000 : 1 (Krause, 1993; Krause et al., 1992). Krause (1993) exposed purple sea urchins to samples of seawater collected at various distances west of the Carpinteria diffuser and found reproductive success decreased as produced water concentration increased. Reproductive success proved useful in inferring produced water concentration in the samples and in detecting toxicity in the environment (Krause, 1993).

These studies are valuable but limited by the spatial and temporal scales resolved. They resolve spatial scales of 1000 m and smaller, but only at a few points and only along isobaths. Thus, the effects of cross-shore dispersion cannot be examined. The shorter duration experiments resolved temporal scales ranging from a few hours to a few days and spanning a limited range of ocean conditions. The longer duration experiments integrated over time scales of a few months to produce single data points. Over these time scales ocean conditions change substantially. Thus, impacts due to shorter time scale processes and variable ocean conditions cannot be identified. These biological studies cannot be used to examine the variations in produced water dispersion on seasonal time scales. Nor can they resolve complex spatial patterns which might arise from variable ocean currents and stratification. Consequently, their usefulness in predicting the effects of produced water is limited.

Our approach to increase the predictability of these studies is to use physical oceanographic observations to define the ambient conditions and then to simulate produced water dispersion with a simple numerical model. Theoretical and experimental studies show that the structure of buoyant plumes is dependent on ambient density stratification and velocity field in the receiving fluid (cf. Fischer et al., 1979; Roberts et al., 1989a–c; Lee et al., 1996; Pritchard et al., 1996; List, 1982; Washburn et al., 1992; Wu et al.1994; Wu, 1993). Thus, observations of evolving stratification and currents around the point of discharge are critical for modeling.

We model the dispersion of produced water as a two step process. In the first step, the buoyant plume rises and mixes with ambient seawater until it reaches an equilibrium level or the sea surface. We refer to the region in which this occurs as the 'near-field'. We simulate near-field mixing by using the buoyant plume model described by Baumgartner et al. (1994) using our time series observations of currents and density as inputs. In a recent study by Petrenko et al. (1998), this model was successful in predicting the height of rise, thickness, and initial dilution of the wastewater plume produced by the sand island treatment plant in Mamala Bay, Hawaii. The second step of the dispersion process occurs in the 'far-field', following plume rise, when ambient mixing and stirring processes further dilute the plume. We simulate these far-field processes with the model for two-dimensional diffusion discussed by Okubo (1980). Spatial patterns of produced water concentration in the far-field are inferred from 'visitation frequency' diagrams constructed from current observations.

Our investigation is motivated by the biological studies conducted around the Carpinteria diffuser that revealed toxic effects as far as 1000 m from the outfall. An underlying hypothesis is that these effects resulted from dissolved components which are carried far from the point of discharge by the spreading plume. The Carpinteria outfall ceased operation shortly after the conclusion of the biological studies and before our field observations commenced. Thus, our work is retrospective and assumes that conditions during the time of our sampling represent prevailing conditions. Specific objectives of our study are: (1) to describe the evolving structure of the water column and currents on seasonal time scales and shorter; (2) to use these observations in modeling the spatial scales of the plume; (3) to estimate dilution levels of produced water around the diffuser; and (4) to interpret the various biological field assays in the light of the observations and model results.

2. Methods

2.1. Field site and instrumentation

The produced water outfall lies off the coast near the Carpinteria, CA at 34° 23′ N, 119° 30.64′ W (Fig. 1). Mean water depth at the diffuser is about 12 m with a ~ 2 m tidal variation. The diffuser, with length $L = 21$ m, is at the end of the outfall pipe that extends about 300 m from the coastline. It consists of seven risers with tee-ports that extend upward off of a central pipe 0.20 m in diameter. Spacing between tee-ports along the diffuser is 3.5 m. The tee-ports discharge effluent horizontally into the water column at $3.2\ \mathrm{m\,s^{-1}}$ through two appositely-directed nozzles, each 0.03 m in diameter. The points of discharge are about $e_{\mathrm{p}} = 1$ m above the sea floor. Diffusers of this type are designed to produce minimum dilutions of order 100 (Fischer et al., 1979). The sea floor around the diffuser is gently sloping and sandy with isobaths oriented about 100° relative to true north (Fig. 1c). About 1 km west of the diffuser is Carpinteria creek which is the discharge channel of the Carpinteria salt marsh.

Profiles of temperature, conductivity and pressure were collected every two weeks, weather permitting, from 29 July 1992 to 4 January 1994 using a conductivity, temperature, depth profiler (CTD, Sea Cat SBE 19 manufactured by Sea-Bird Electronics Inc., Bellevue WA). Thirty four profiles were obtained at the diffuser and at four nominal locations around it: 100 m east, 100 m west, 100 m inshore, and 100 m offshore. Time-depth contours of temperature, salinity and density from all 5 locations are very similar and only results when the diffusers are presented. Data from downcast profiles are averaged over 0.5 decibar (dbar) and used for computing salinity and density. Reliable data were not consistently obtained in the upper 1 m so this portion of the water column is not included in the analysis.

Current magnitude and direction were measured by mooring two electromagnetic current meters (model S4, manufactured by InterOcean Inc., San Diego, CA) 25 m west of the diffuser along the 12 m isobath. One current meter was moored 5 m from the bottom (approximately 7 m depth), and the other 1m from the bottom (approximately 11 m depth). The upper depth was chosen to obtain data in the mid-water column, but avoid heavy boat traffic in the area. Data from two different pairs of S4

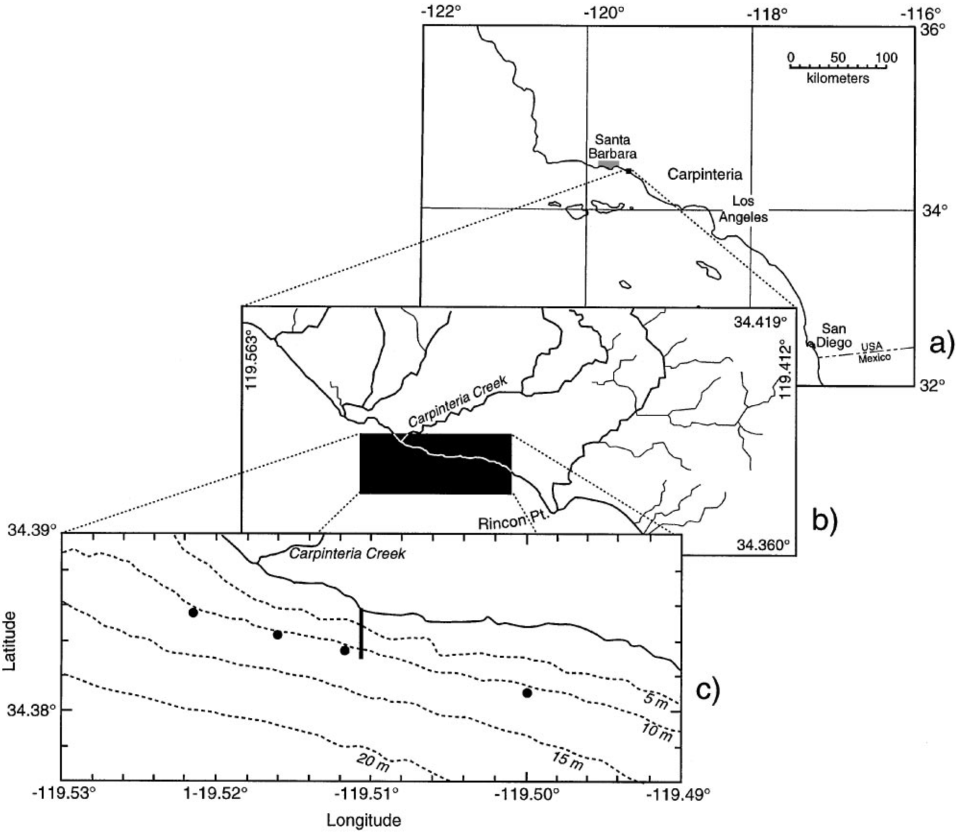

Fig. 1. (a) Area map of Southern California showing field site near Carpinteria, CA. (b) Map of coastline and watershed around the field site. (c) Field site showing produced water discharge pipe and diffuser (heavy line) and bathymetric contours (dotted lines). Dots indicate biological moorings at 100, 500 and 1000 m west of the diffuser and 1000 m east of the diffuser.

current meters are reported. The first was deployed from 20 December 1992 to 16 April 1993 and the second from 13 July 1993 until 3 January 1994. For all deployments the current meters were configured to collect 2 min vector averages of currents every 20 min, giving a sampling frequency of $f_s = 72$ cycles day^{-1}. Further discussion on the CTD, current meter, and data processing is given by Stone (1995).

2.2. Modeling near-field dispersion

In the near-field, produced water initially disperses as a rising buoyant plume which we simulate using the plume model described by Baumgartner et al. (1994). The model is specifically designed to simulate buoyant plume discharge from multi-port diffusers in stratified cross flows, like the one at Carpinteria. The model (hereafter referred to as the RSB model) is based on laboratory experiments described by Roberts et al.

(1989a–c) and on dimensional analysis. Plume dispersal was examined over a wide range of stratification conditions and current speeds using small model diffusers similar in configuration to the Carpinteria diffuser. Results were summarized by a series of equations with non-dimensional parameters which are used in the RSB model to predict plume characteristics.

Model inputs are the diffuser characteristics along with current speed and density profiles. For each of the 34 density profiles collected at the diffuser, we made 4 model runs at current speeds of 0, 0.5, 0.1, and 0.2 m s^{-1} for a total of 136 model runs. The chosen speeds span 99% of the range of measured current speeds. We assume that current vectors are perpendicular to the diffuser, consistent with the prevailing along-isobath flow at the site. Density data are edited to remove inversions which typically occurred during periods of weak stratification and are probably instrumental artifacts. Density at 10 levels is used for each model run and the water depth was assumed constant at $D = 12$ m.

Among the model outputs are: (1) height of the top of the plume above the discharge depth z_e; (2) plume thickness h_e,; (3) minimum initial dilution S_m; (4) height z_m corresponding to S_m; and (5) length of the 'initial mixing zone' x_i (Fig. 2). These outputs are positive and naming conventions are those used by Baumgartner et al. (1994). For graphical display of plume position in the water column we show: (1) depth of the top of the plume $z_t = z_e + e_p - D$; (2) depth of the bottom of the plume $z_B = z_t - h_e$; and (3) depth of minimum initial dilution $z_c = z_m + e_p - D$. The quantities z_t, z_b, and z_c are negative and z is positive upward from the sea surface.

The position of the plume in the water column, described by z_t and z_b, determines the depth interval over which organisms can be exposed to produced water.

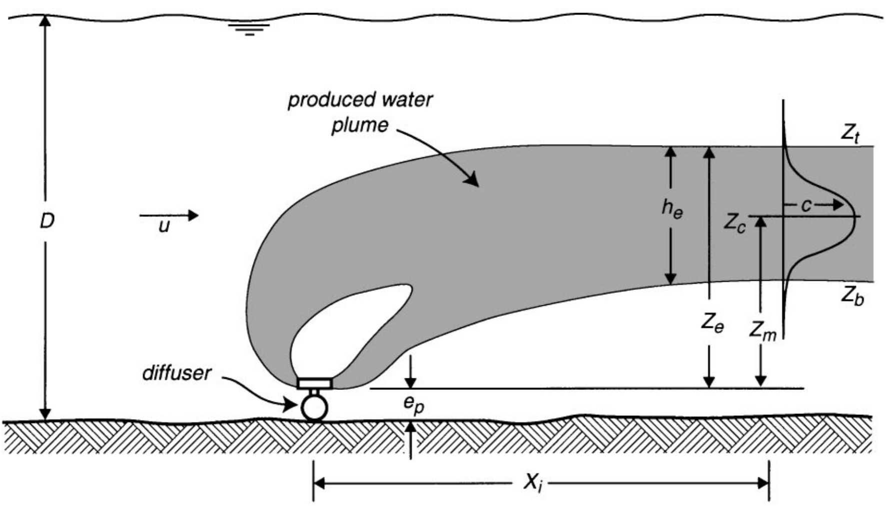

Fig. 2. Diagram of a buoyant produced water plume released from a multi-port diffuser on the seafloor (adapted from Baumgartner et al., 1994). Produce water is discharged through tee-ports on diffuser and spreads as a buoyant plume. See text for explanation of symbols.

Stratification and current speed are primary controlling factors: weak stratification and strong currents increase the interval while strong stratification and weak currents decrease it (Fischer et al., 1979, List, 1982, and Koh and Brooks, 1975). Initial dilution S_m is a measure of the maximum produced water concentration to which organisms are exposed. Dilution is defined as the volume of a seawater sample divided by the volume of produced water in that sample. Weak stratification and high current speeds increase S_m; high stratification and weak currents decrease S_m.

The length of the initial mixing zone x_i, is the horizontal distance over which the plume is advected by ambient currents as it rises, buoyantly mixes, and entrains ambient seawater. In laboratory experiments, Roberts et al., 1989b show that the minimum dilution over plume cross-sections increases rapidly near the diffuser. As distance from the diffuser approaches x_i, the turbulence in the plume quickly collapses and further dilution due to plume-generated turbulence ceases. At distance x_i away from the diffuser, the produced water forms a passive layer within its equilibrium depth range and the minimum initial dilution is S_m at height z_m. Within the layer the concentration of produced water C is idealized as a Gaussian distribution (Fig. 2). Organisms residing within the plume in the initial mixing zone are exposed to highly variable concentrations of produced water due to strong turbulence. Dilution levels can be less than S_m within this zone. Beyond x_i the plume moves into the 'far-field'.

2.3. Modeling far-field dispersion

After the initial mixing during plume rise, ambient ocean mixing processes further dilute the produced water plume and alter its width and height. These complex processes include small-scale turbulent mixing, shear dispersion, and horizontal mixing. In addition, the width of the plume slowly increases and the thickness h_e slowly decreases due to gravitational collapse of the plume into the stratified surroundings (Roberts et al., 1989b). We do not have sufficient measurements to establish the details of how these processes affect the plume. However, we can examine the net effects of these processes on dilution through a simple horizontal diffusion model. In doing so, we assume that horizontal mixing processes are dominant and that the complex dispersion processes can be parameterized by a horizontal eddy diffusivity k_H. Clearly this is an over simplification. The objective here is only to establish the order of magnitude of additional dilution in the far field.

We estimate the far-field dilution with an elementary solution of the two-dimensional diffusion equation. The plume in the far-field is idealized as consisting of a sequence of cylindrical patches of produced water that continuously expand due to two-dimensional mixing processes. The patches move along horizontal trajectories defined by progressive vector diagrams (PVDs) that are obtained from current measurements. PVDs are idealizations of real trajectories since they assume a 'frozen' velocity field (equivalent to the ocean moving as a slab). Nevertheless, they are useful in predicting displacements of water parcels from single point current measurements. We employ 'visitation frequency diagrams' (described below), formed from the PVDs, to examine the spatial distribution of produced water around the diffuser.

The concentration C of a dissolved substance in a circular patch that is diffusing horizontally in a homogenous fluid can be written as (Okubo, 1980 and Fischer et al., 1979),

$$C(r, t) = \frac{M}{2\pi h k_H t} \exp\left(-\frac{r^2}{4k_H t} \right), \tag{1}$$

where M is the total mass of dissolved substance and r is distance from the patch center. In Eq. (1) it is assumed that only horizontal mixing is important, C is uniform over the patch height h, and the concentration of the dissolved substance is zero far from the patch. For simplicity we assume that when the plume enters the far-field at t_o, the horizontal distribution of concentration has a Gaussian shape described by Eq. (1) with standard deviation $(4k_H t_o)^{1/2} = L/2$. This is equivalent to assuming the plume width is of the same order as the diffuser length. This assumption is supported by the laboratory findings of Roberts et al. (1989b) in which the width of the plume at x_i was in the range 1.3–1.6 L, although there is considerable scatter in their data (see for e.g. Fig. 10). Evaluating Eq. (1) at $r = 0$, the ratio of the concentration of produced water in the center of the patch at time t_o to the concentration at $t_o + t$ yields the relative dilution,

$$S_f(t) = \frac{C(0, t_o)}{C(0, t)} = l + \frac{t}{t_o} = l + t\left(\frac{16k_H}{L^2}\right). \tag{2}$$

Okubo (1980) shows that k_H varies approximately as $k_H \propto l^{4/3}$ (with wide scatter) for ocean data where l is the horizontal scale of the mixing phenomena (his Fig. 2.4). We estimate a range of diffusivities, $5 \times 10^{-2} \leqslant k_H \leqslant 6 \times 10^{-1}\ \mathrm{m^2\,s^{-1}}$ corresponding to horizontal scales of a order 100–1000 m. We take this to be representative of horizontal mixing scales between the diffuser length (21 m) and the distance to the farthest biological test sites (1000 m). For the time scale t in Eq. (2) we use an advection time based on the visitation frequency diagrams.

To estimate the spatial distribution of produced water in the far-field around the diffuser, we calculate visitation frequency (VF) diagrams (Roberts, 1990 and Baumgartner et al., 1994) from the current meter data at 7 and 11 m. As described above, the plume is imagined to consist of a sequence of patches of produced water. These emerge from the diffuser at time intervals δt corresponding to the times of current measurement (every 20 min). Each PVD is computed over a specified integration time T'. To include tidal effects we use $T' = 24$ h. The position of the PVD at each δt is sorted into the spatial bins of a 2-dimensional histogram. This consists of an x–y (east–north) grid of bins around the diffuser: 4000 along the x-axis and 2000 along the y-axis. The bin size is $\Delta x = 20$ m and $\Delta y = 20$ m, corresponding to the approximate length of the diffuser. PVD's begin at the time of each data point in the current time series and are integrated for T'. VF is computed for the longest continuous current record (22 December 1992 to 16 April 1993; 2732 h). After sorting, the number of points in each bin n_j is normalized by the total number of data points N in the current record to give VF: $\mathrm{VF}_j = n_j/N$. VF is contoured to simulate patterns of plume dispersion. The isopleths of VF estimate the fraction of time the plume is found at locations around the diffuser. For each bin, the mean advection time t_j from the diffuser to the bin is also computed. t_j is used as the time scale t in Eq. (2) to compute $S_f(t)$ around the diffuser.

3. Results

3.1. Water column evolution and near-shore currents

The CTD observations at the diffuser show two distinct thermal regimes through the year: (1) the summer regime from May through September, characterized by strong thermal stratification; (2) the winter regime from October to April, characterized by weak thermal stratification (Fig. 3a). The water column was thermally

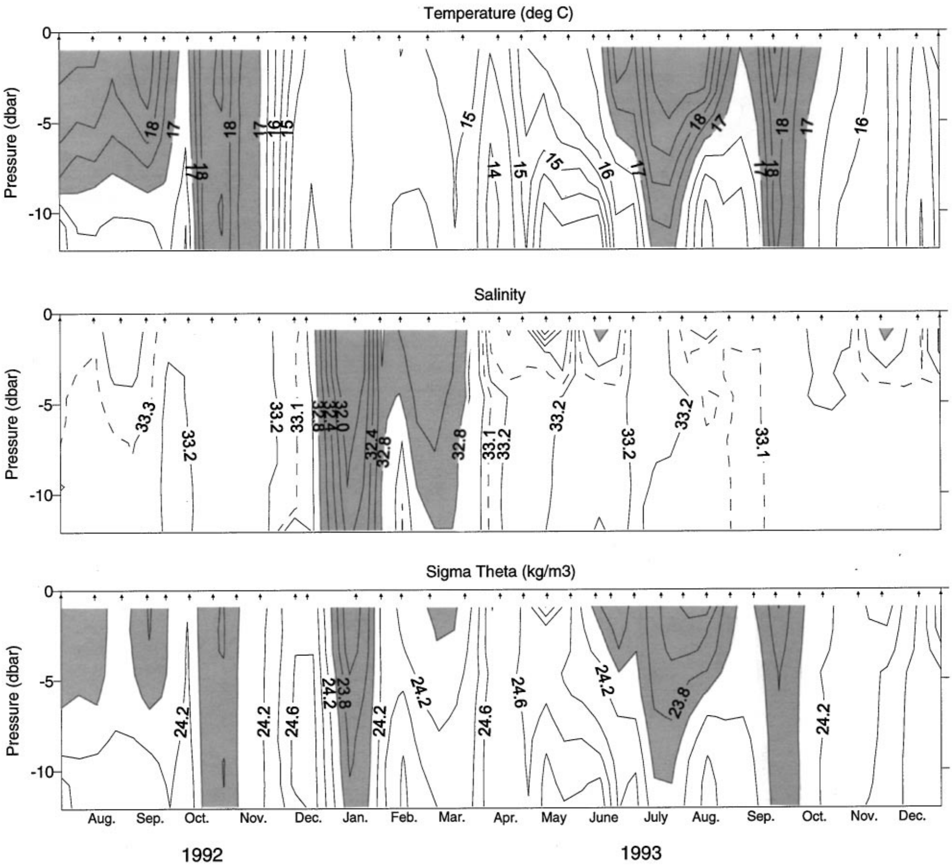

Fig. 3. Time-depth contours of (a) temperature (contour interval is 0.5°C), (b) salinity (contour interval is 0.2 between solid lines; additional contours shown as dashed lines), (c) potential density anomaly σ_θ (contour interval is 0.2 kg m^{-3}). Shaded areas are warmest temperatures, lowest salinities, and lowest densities. Arrows along the upper axis in each panel show the times of CTD casts. Data were not reliably collect in the upper 1 dbar and results are not shown here.

stratified when our measurements commenced on 29 July 1992. Cooling began in September, but thermal stratification persisted throughout the month. By mid-October thermal stratification weakened as the water column became nearly isothermal. Salinity decreased slightly to 33.2 psu during this period, indicating advection of a new water mass (this change is not resolved by contours spacing of Fig 3b). Between sampling on 27 October 1992 and 22 December 1992, the water column cooled from 18°C to 14°C and the potential density anomaly (σ_θ) increased from about 24.2 kg m^{-3} to 24.6 kg m^{-3} (Fig. 3c). Winter rainfall produced large increase in density stratification at the field site (Fig. 3c) with layering of fresh water most prominent in January, February, and March, 1993 (shaded areas, Fig. 3b). During these times moderate stratification prevailed even though the water column was nearly isothermal (Fig. 3a). On 20 January, 1993, for example, σ_θ increased from 23.130 kg m^{-3} at 1 dbar to 23.795 kg m^{-3} at 11 dbar. The mean buoyancy frequency then was $N = 13.2$ cycles/h (cph) where,

$$N = \left[-\frac{g}{\rho}\frac{\partial \rho}{\partial z} \right]^{1/2} = \left[-\frac{g}{\rho}\frac{\Delta \rho}{\Delta z} \right]^{1/2}. \tag{3}$$

g is the gravitational acceleration, ρ is seawater density, and z is positive upwards. N is computed from the density difference $\Delta\rho$ over the entire measurement depth Δz, typically 11 m.

After the period of rainfall, weaker thermal stratification prevailed until June, 1993 when stratification increased. The maximum stratification observed occurred on 21 June 1993 when the temperature varied from 18.6°C at 1 m to 15.9°C at 11 m with $N = 22$ cph. Strong thermal stratification persisted until October, 1993 when the water column cooled and became more uniform. By 11 October 1993, the water column was nearly isothermal again with a temperature of 17.5°C. In November and December the water column remained nearly isothermal and cooled from 16°C to less than 15°C.

Currents are highly variable at the field site throughout the year and at both measurement depths, nominally 7 and 11 m (Fig. 4). However, no clear seasonal trend in currents is found in our records. Sub-tidal currents show low frequency events in which currents are fairly steady for periods of a few days (data not shown). Little coherence is evident between sub-tidal current velocity at 7 and 11 m and large differences in speed and direction frequently occur. A representative subset of the current data (Fig. 4) shows periodicity in the current time series resulting primarily from the semi-diurnal, lunar (M_2) tide. Power spectra of current speed at 7 and 11 m show clear peaks at the M_2 frequency (data not shown). Nearshore current observations from other locations in the Southern California Bight also show the dominance of the M_2 tide. For example, Winant and Olson (1976) reported 0.1 m s^{-1} along-shore currents due to the M_2 tide at 18 m depth off Del Mar, CA.

Histograms of current direction at 7 and 11 m exhibit very different distributions. At 7 m the histogram of current direction has two clearly defined peaks, one around 100° and another around 280° (Fig. 5a). These directions are approximately parallel to

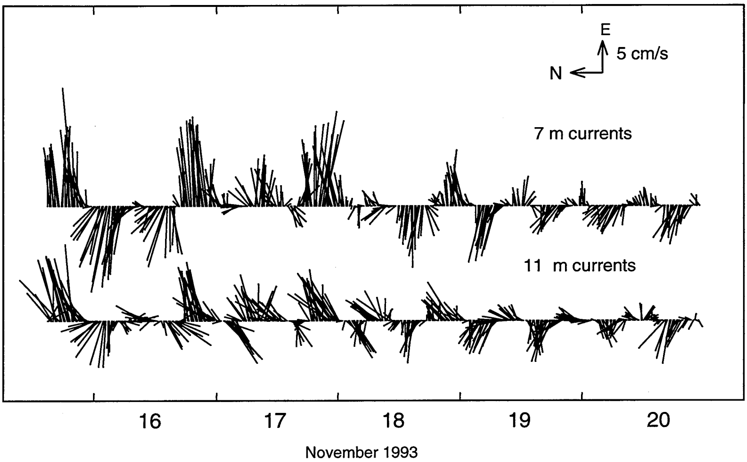

Fig. 4. Needle plots of current magnitude and direction at 7 m (upper time series) and 11 m (lower time series) for 16–20 November 1993. Each needle represents a 2 min vector average of a current velocity and needles are 20 min apart. Speed scale shown in upper right corner.

depth contours (Fig. 1c) and indicate along-isobath flow. At 11 m the histogram exhibits a single broad maximum at around 270° (Fig. 5b) and no clear peak is found around 100°. Totals in bins at 0, 90, 180, 270 degrees have been set to zero in the histograms of Fig. 5. Anomalous high values in these bins result from uncertainties in current direction at speeds of less than 2 cm s^{-1} (Stone, 1995). Table 1 shows that the flow distributions sorted by quadrant change significantly between 7 and 11 m. Southward (cross-isobath) flow is much more common at 11 m (28.8% of record) than at 7 m (8.3%). Westward flow occurs most frequently at both depths: for 33.7% of the 11 m record and for 43.4% of the 7 m record.

Given the high variability in current speed, the produced water plume can be significantly affected by currents. The effects of currents may be parameterized by the Froude number for buoyant plumes (Fischer et al., 1979),

$$F = \frac{u^3}{b}, \tag{4}$$

where u is current speed and b is the specific buoyancy flux. Specific buoyancy flux is,

$$b = g\frac{(\rho_0 - \rho_e)}{\rho_0}\frac{Q}{L}, \tag{5}$$

where ρ_o is ambient density, ρ_e is produced water density, and Q is volume flux from the diffuser. F is the ratio of the flux of kinetic energy of the mean flow to the buoyancy flux of the plume. High values of F lead to a diffuse plume because currents mix more ambient fluid into the plume (Fischer et al., 1979, Roberts et al., 1989a). Low values of F result in a more concentrated plume because advection is weaker and less ambient

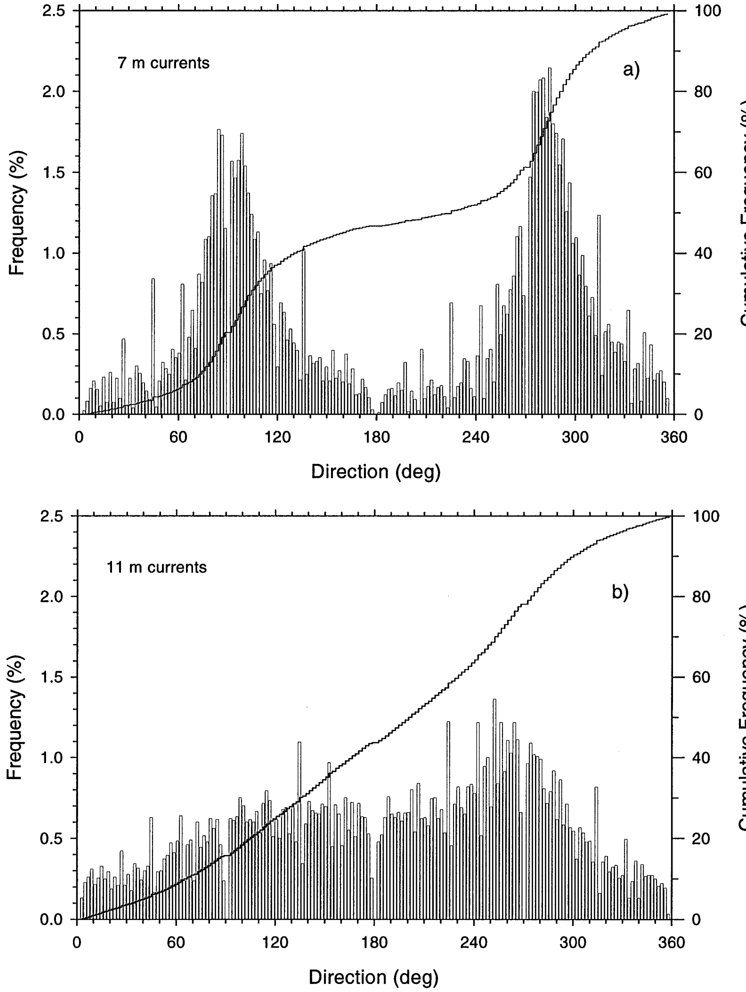

Fig. 5. (a) Histogram of current direction for 7 m data (left hand scale). Increasing curve shows cumulative frequency (right hand scale) Total of 17,337 points sorted. (b) As in (a) but for 11 m current direction. Total of 17,972 points sorted. Bin width is 2° in both histograms.

fluid mixes with the rising plume. Discharge records of produced water characteristics and Q for the Carpinteria diffuser yield an average of $b = 1.564 \times 10^{-4}\,\mathrm{m^3\,s^{-3}}$. Specific buoyancy flux is computed using a typical daily value of $Q = 2.64 \times 10^6$ $l\,\mathrm{day}^{-1}$ (6.97×10^6 gal day^{-1}). Modeled values of b change slightly through the year due to variations in ρ_o. Daily discharge volumes were obtained from records kept at the produced water processing plant at Carpinteria (William Ford of Chevron, Inc., personal communication, 1994).

Measured current speeds range from 0 to $0.47\,\mathrm{m\,s^{-1}}$ with $u \leqslant 0.1\,\mathrm{m\,s^{-1}}$ for 90% of the record and $u > 0.2\,\mathrm{m\,s^{-1}}$ for 1% (Fig. 6). F ranges from 0 to 648 with $F \leqslant 1$ for

Table 1
Current statistics at the Carpinteria site

	7 m currents				11 m Currents		
Quadrant	Direction (deg)	No. observations	% of record	speed ($m\,s^{-1}$)	No. observations	% of record	speed ($m\,s^{-1}$)
East	45–135	6607	38.1	0.05	4575	25.5	0.05
West	225–315	7522	43.4	0.06	6060	33.7	0.05
South	135–225	1442	8.3	0.02	5178	28.8	0.04
North	315–45	1766	10.2	0.02	2159	12.0	0.03
	Total	17337	100		17972	100	

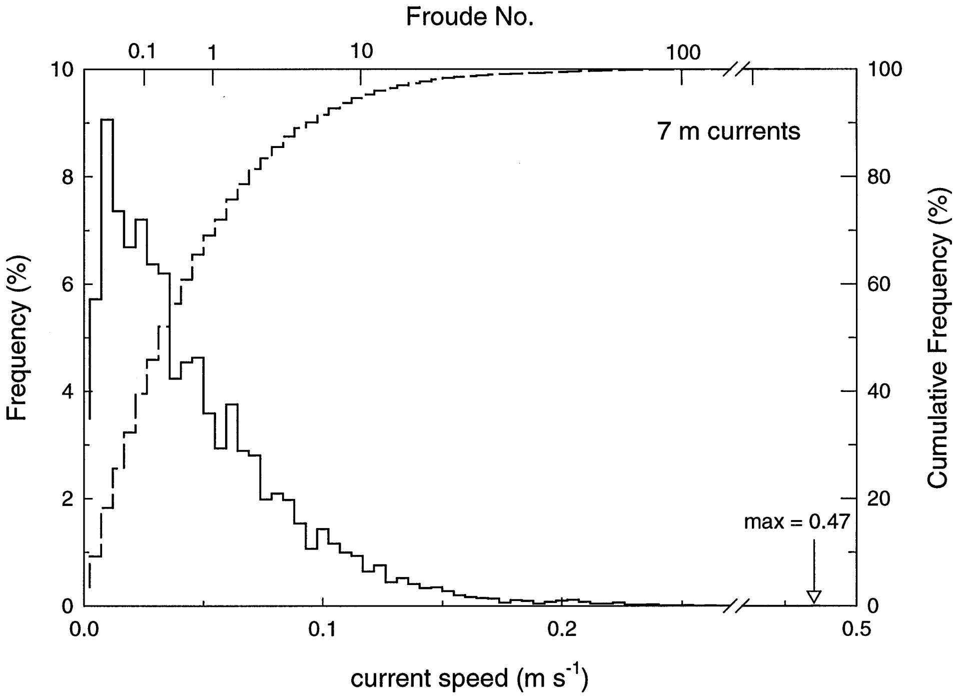

Fig. 6. Histogram (solid line, left hand scale) and cumulative distribution (dashed line, right hand scale) of current speed u at 7 m. Upper scale shows corresponding values of Froude number $F = u^3b^{-1}$ based on the mean specific buoyancy flux $b = 1.56 \times 10^{-4}\,m^3\,s^{-3}$.

68% of the record and $F > 10$ for 5%. For $F \leqslant 0.1$, about 33% of the record, the plume structure is similar to that found in a stationary environment (Roberts et al., 1989a). Similar ranges of u and F are found at 11 m (data not shown). The broad range of F indicates that the plume structure changes depending on the current regime.

3.2. Near-field mixing

The modeled position of the plume in the water column is strongly modulated by changing stratification through the year (Fig. 7a–c). This occurs for all modeled current speeds and the results of Fig. 7 for 0 and 0.1 m s^{-1} are representative. The modeled plume is lowest (minimum z_t) and thinnest (minimum $z_t - z_b$) during the periods of highest stratification in summer. For 1993 this happens in June when $z_t = -6.5$ m and $z_t - z_b = 2.6$ m. The depth of the bottom of the plume z_b is more constant than z_t due to entrainment of deeper, denser waters. It is always more than 7 m from the surface, but seldom within 2 m of the bottom. The depth of minimum initial dilution lies above the mid-point of the plume and its depth varies more than z_t and less than z_b. In the period January through March, 1993 the plume depth first decreases, then increases, and then decreases again due to changing salinity stratification from rainwater runoff (Fig. 3).

The effect of current speed on plume depth is clearly evident: at zero current speed the plume rises higher into the water column at all stratifications. In late fall and early

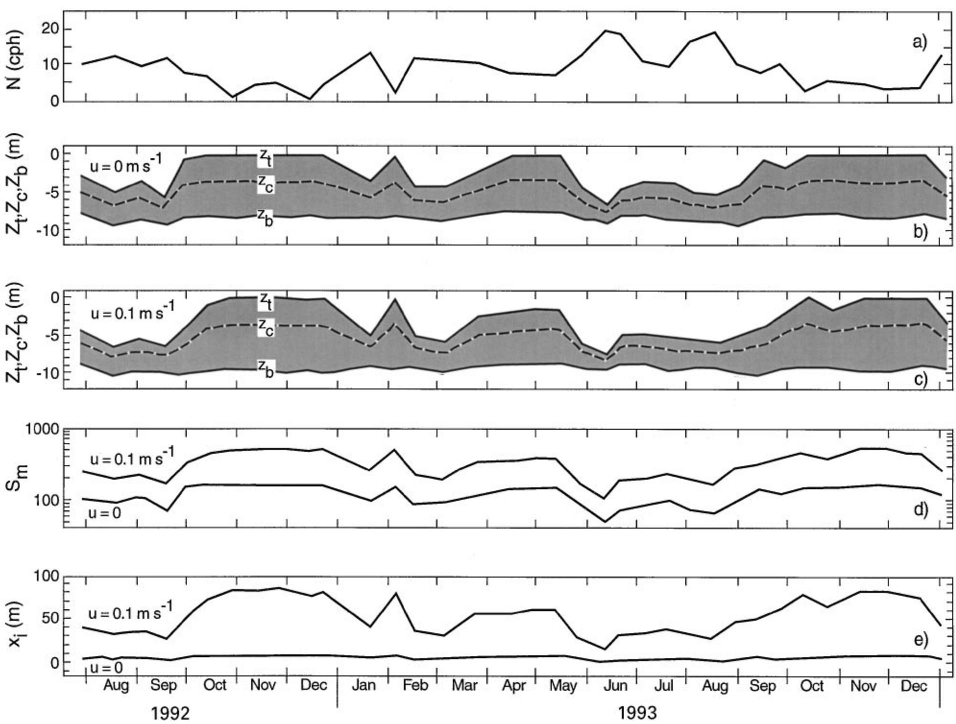

Fig. 7. Near-field modeling of produced water plume. Panels show outputs from RSB plume model based on time series of density shown in Fig. 3c. (a) Plume depths with $u = 0$ m s^{-1}. Lower solid line shows bottom of plume (z_b), upper solid line shows top of plume (z_t), and dashed line shows depth of minimum dilution (z_c). (b) As in (a) but for $u = 0.1$ m s^{-1}. (c) Minimum dilution in plume at current speeds of 0 m s^{-1} (lower curve) and 0.1 m s^{-1} (upper curve). (d) Length of initial mixing zone for 0 m s^{-1} (lower curve) and 0.1 m s^{-1} (upper curve).

winter (October into December) the plume surfaces and occupies most of the water column for $u = 0$ (Fig. 7b). A shorter period of plume surfacing occurs in April and May, 1992. At $u = 0.1\ \mathrm{m\,s^{-1}}$, z_t is deeper in the water column and the plume surfaces for shorter periods in winter (Fig. 7c). Overall, however, the effects of currents are less important in controlling the plume height than stratification.

Another consequence of changing stratification and current speed is that the minimum initial dilution S_m is highly variable. When stratification is high in summer and after rain events in winter, the plume is mixed over less of the water column (reduced $z_t - z_b$) resulting in lower values of S_m. For example, with $u = 0$, $S_m = 50$ in mid-June 1993 (Fig. 7d); with $u = 0.1\ \mathrm{m\,s^{-1}}$, $S_m = 100$ at this time. For periods of weaker stratification in fall and winter, the plume mixes over more of the water column and S_m is higher. At these times, maximum $S_m \approx 150$ for $u = 0$ and $S_m \approx 500$ for $u = 0.1\ \mathrm{m\,s^{-1}}$.

The extent of the initial mixing zone x_i is a strong function of both current speed and stratification (Fig. 7e). For $u = 0$, x_i is fairly constant at 10 m or less. At $u = 0.1\ \mathrm{m\,s^{-1}}$, x_i varies from a minimum of about 20 m in summer to over 80 m in winter. Freshwater stratification from winter storms reduces x_i to around 30 m on time scales of less than a few weeks. After the storms, x_i quickly increases as stratification decreases.

3.3. Far-field mixing

The VF diagram computed from currents at 7 m indicates a strong tendency for the produced water plume to advect along shore (i.e. follow isobaths) in mid-water column (Fig. 8a). The pattern of isopleths is roughly symmetric along shore and across shore, but the along-shore scale of the pattern is about six times the cross-shore scale. At 11 m the along-shore scale of isopleths is reduced compared with 7 m and the pattern is displaced offshore (Fig. 8b). The pattern indicates that produced water near the bottom would frequently advect offshore, toward the southwest. The presence of non-zero values inshore of the coastline is an artifact of the assumption of frozen flow. Velocity gradients may exist inshore of the current meter positions and are not represented in the PVD's.

Dilution in the far-field ranges from minimum values, which we can estimate, to essentially infinite values when uncontaminated seawater is present. We estimate the total far-field dilution at 7 m when the plume is present by,

$$S_{\Delta t} = S_m S_f, \tag{6}$$

where subscript Δt denotes that the plume is present for time Δt out of a total record length T. Advection time t, used for computing S_f from Eq. (2), ranges from ~ 3 h at 100 m from the diffuser to 10–12 h at 1000 m (contours of t not shown). Lowest $S_{\Delta t}$ is likely in summer when S_m is small. Assuming minimum $S_m \approx 50$ (Fig. 7d) and low $k_H \approx 0.05\ \mathrm{m^2\,s^{-1}}$, $S_{\Delta t}$ ranges from 500 for the mooring 100 m west of the diffuser to 3000–4000 at the 1000 m moorings (Fig. 9A). During weakly stratified conditions common in winter, $S_{\Delta t}$ is much higher: with $S_m \approx 500$ (Fig. 7d) and high

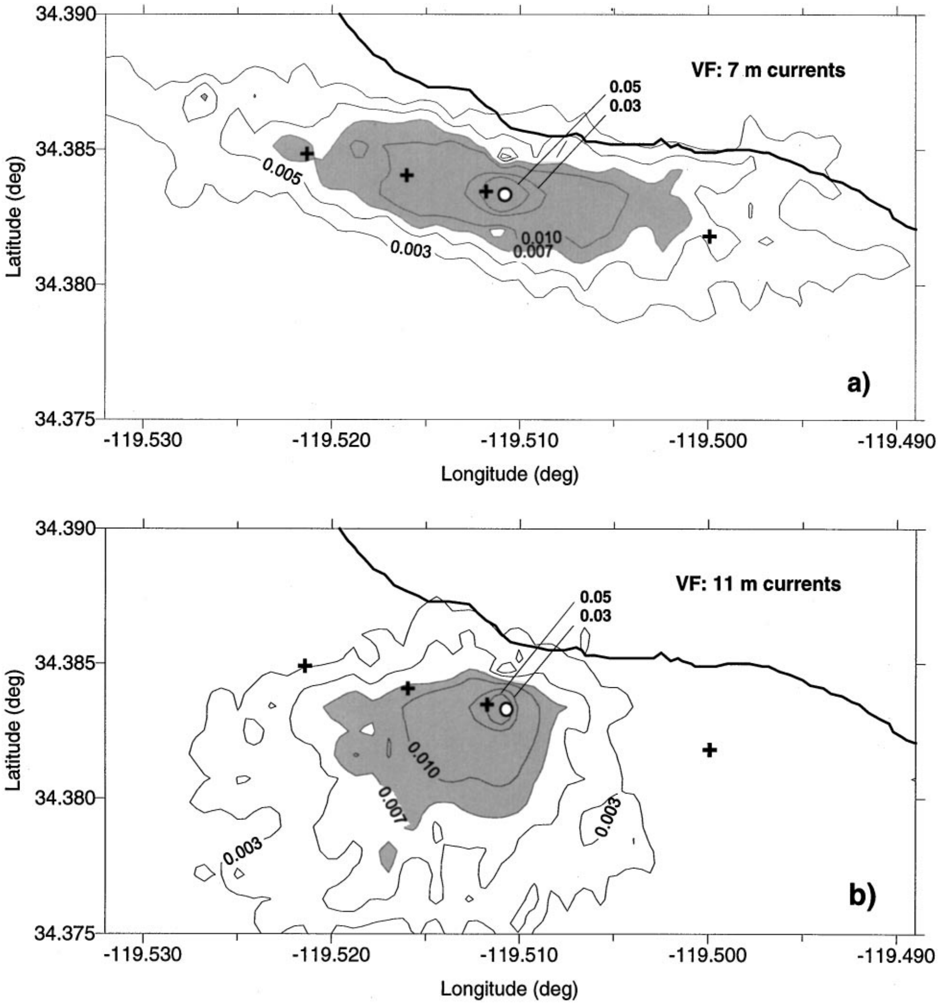

Fig. 8. (a) Diagram of visitation frequency VF indicating fraction of time that plume is present at locations around the diffuser. VF computed from currents at 7 m. Only values above 0.003 are shown and those above 0.007 are shaded. Plus signs (+) show locations of biological moorings 100, 500 and 1000 m west of the diffuser and 1000 m east of the diffuser. Location of produced water diffuser indicated by white dot in center of pattern. Coast line indicated with heavy solid line. (b) As in (a) but for VF computed from currents at 11 m.

$k_H \approx 0.6\ \mathrm{m^2\,s^{-1}}$, $S_{\Delta t}$ at the moorings is 1–5 $\times$ 10^5 (Fig. 9B). We have no data indicating a seasonal dependence of k_H. However, we use a low and high values for summer and winter conditions to determine the maximum range in expected dilution. Clearly, uncertainty in k_H is an important source of error in these dilution estimates.

Time-averaged dilution S_T is much higher than $S_{\Delta t}$ because the plume is not present at any point in the far-field for all T. Following Fischer et al. (1979), S_T is obtained

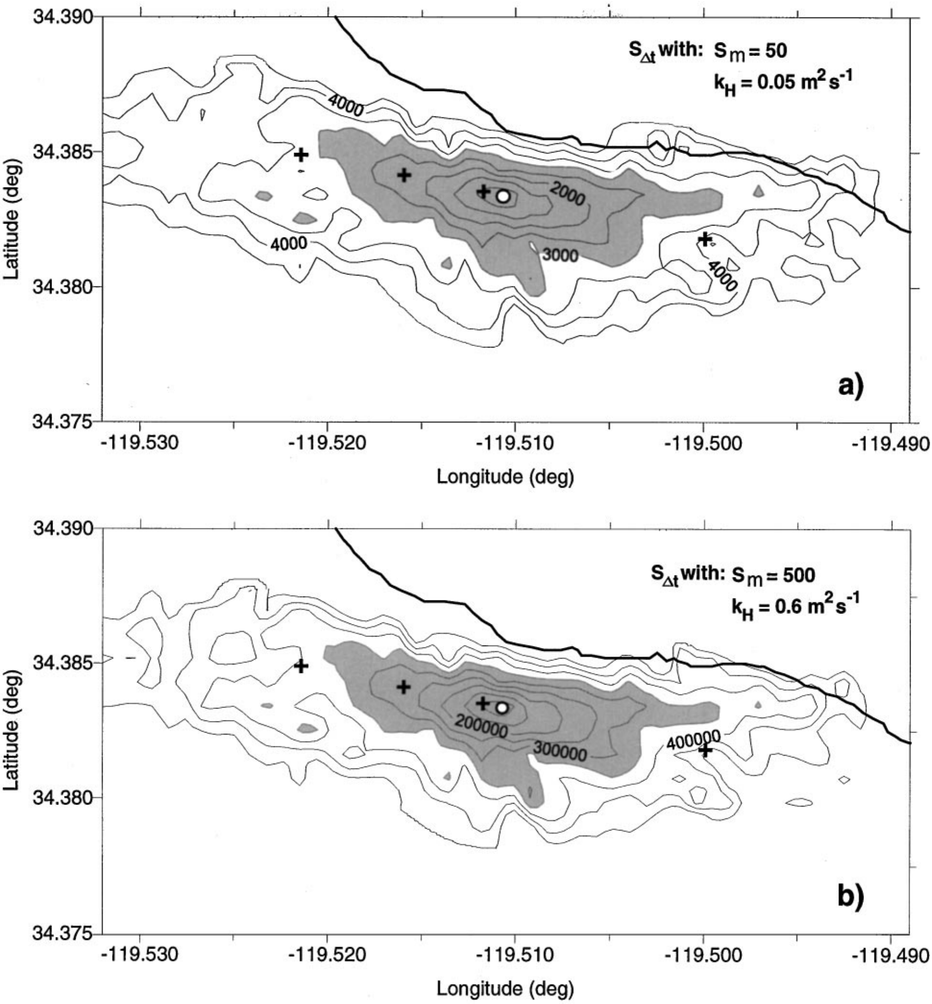

Fig. 9. (a) Dilution in far-field $S_{\Delta t}$ at 7 m depth when plume is present. $S_{\Delta t}$ is computed for summertime conditions, assuming near-field dilution $S_m = 50$ and horizontal eddy diffusivity $k_H = 5 \times 10^{-2}\,m^2\,s^{-1}$. $S_{\Delta t}$ shown for visitation frequencies above 0.003. Areas with $S_{\Delta t} < 3000$ are shaded. Contour interval is 500. (b) As in (a) but for wintertime conditions assuming $S_m = 500$ and $k_H = 6 \times 10^{-1}\,m^2\,s^{-1}$. Contour interval is 10^5.

from the time-averaged, relative concentration $C_T = S_T^{-1}$, where:

$$C_T = T^{-1} \int_0^T C(t)\,dt = C_{\Delta t} \frac{\Delta t}{T} \tag{7}$$

and $C_{\Delta t} = S_{\Delta t}^{-1}$ is the average relative concentration when the plume is present. Substituting

$$S_T = S_{\Delta t} \frac{T}{\Delta t}, \tag{8}$$

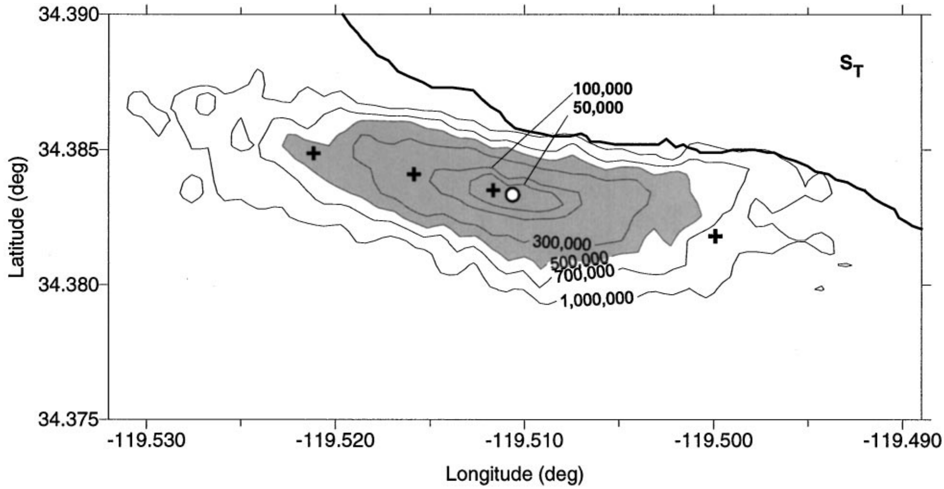

Fig. 10. (a) Time-averaged dilution in far-field S_T at 7 m depth. S_T is computed for summertime conditions, assuming near-field dilution $S_m = 50$ and horizontal eddy diffusivity $k_H = 5 \times 10^{-2}\,m^2\,s^{-1}$. S_T shown for visitation frequencies above 0.003. Time-averaged dilutions for wintertime conditions are 1–2 orders of magnitude larger (not shown).

we estimate S_T from $S_{\Delta t}$ (Fig. 9) with $\Delta t/T$ approximated by the visitation frequency at 7 m (Fig. 8a). The resulting spatial distributions of S_T vary widely within 1000 m of the diffuser (Fig. 10). For summertime conditions and low k_H, S_T ranges from 3×10^4 at 100 m from the diffuser to $5–7 \times 10^5$ at 1000 m (Fig. 10). For wintertime conditions S_T is much higher: $S_T \sim 10^6$ at 100 m from the diffuser and $S_T \sim 10^8$ at 1000 m (not shown).

4. Discussion

Results from our study of produced water dispersion are consistent with results from the biological studies conducted at the Carpinteria site. Raimondi and Schmitt (1992) found that larvae of red abalone were adversely affected by proximity to the diffuser at all depths tested (1.5 m from surface and 1.5 m from bottom). Because their experiments were conducted in October when stratification is weak, it is likely that produced water extended over most of the water column (Fig. 7b and c). Surfacing of the plume also occurs in October based on our modeling. Thus, it would be expected that larvae moored near the surface around the diffuser would be exposed frequently to produced water.

The decrease in toxic effects away from the diffuser is consistent with the decrease in VF (Fig. 8a), increased $S_{\Delta t}$ (Fig. 9), and increased S_T (Fig. 10). Moorings of Raimondi and Schmitt (1992) at 5, 10, and 50 m were often within the modeled initial mixing zone which typically extends 10–80 m away from the diffuser (Fig. 7e). Organisms in the initial mixing zone would experience highly variable dilution levels due to mixing processes in the rising plume. Instantaneous dilution could often be much less than S_m of Fig. 7d. This may account for the 50% survivorship of pre-competent larvae within 10 m of the diffuser and a 70% survivorship at 100 m. The isopleths of VF at 7 m suggest that the mooring 100 m west of the diffuser is exposed to produced water about 5 times more frequently than the mooring at 500 m and ~ 7 times more than the one at 1000 m (Fig. 8a). The east–west symmetry in the pattern of toxic effects noted by Raimondi and Schmitt (1992) agrees with the symmetric pattern of visitation frequency of Fig. 8a.

The toxic effects near the bottom found by Raimondi and Schmitt (1992) appear to contradict some the model results for near-field dispersion of the plume. In Figs. 7b and c the base of the plume is seldom within 2 m of the bottom, so organisms at 1 m would not necessarily be exposed to the produced water. However, we speculate that the turbulent bottom boundary layer may often extend into the plume. Under these circumstances, produced water could be entrained and mixed downward below the plume's equilibrium depth range. Alternatively, at high current speeds in the 'forced entrainment' regime (Roberts et al., 1989a), the base of the plume remains at the port depth (1 m) over the entire initial mixing zone. When this happens, organisms 1 m above the bottom and within the initial mixing zone would be exposed directly to produced water. Roberts et al. (1989b) found that the minimum value of Fr corresponding to forced entrainment occurs somewhere in the range $1 < \mathrm{Fr} < 10$. Based on our measured current speeds, the forced entrainment regime prevails 5–32% of the time at the Carpinteria site.

Osenberg et al. (1992) found that sub-lethal effects on mussels and pre-competent larvae increased with proximity to the diffuser and exhibited east–west symmetry. Again, the patterns are consistent with our results. The mussels were placed 4.5 m above the bottom, a depth almost always within the equilibrium depth range of the plume (Fig. 7b and c). Thus, very frequent exposure to produced water could occur, particularly for moorings near the diffuser. Exceptions would be during very brief periods of strong stratification and high currents when the plume is deeper in the water column (e.g. June 1993, Figs. 7b and c). Under stratified conditions, common in summer when the plume is trapped at depth, organisms near the surface would not be exposed to produced water, even directly over the diffuser.

These model results support the conclusion of Krause (1993) that the plume extends at least 1000 m from the diffuser. They also suggest that measurable toxic effects may extend beyond 1000 m from the diffuser. Krause (1993) derived a profile of produced water concentration west of the diffuser based on toxicity. From samples collected in May, 1991 at 1000 m west of the diffuser, he estimated a relative concentration of 2×10^{-6}, equivalent to a dilution of 5×10^5. This is close to the (very broad) range of $S_{\Delta t}$ from our modeling (Fig. 9): at 1000 m west of the diffuser $S_{\Delta t}$ is 4×10^3–4×10^5, depending on S_m and k_H. Krause (1993) found up to a 10% reduction in the fertilization of purple sea urchin eggs when sperm were exposed to produced water concentrations as low as 0.0001% (relative dilution of 10^6). Based on our modeling, $S_{\Delta t}$ typically exceeds this threshold (Fig. 9). During periods of high stratification common in summer, S_T also exceeds this threshold (Fig. 10). For conditions of weak stratification common in winter, S_T is $\sim 10^6$ at 100 m and much larger beyond, so toxic effects are likely to be less widespread.

Our results suggest the following predictions concerning the spatial distribution of produced water at the Carpinteria site:

1. East–west (along-isobath) symmetry in the distribution of produced water is maintained throughout the year in the mid and upper water column.
2. The spatial scale of the along-shore distribution of produced water is about 6 times the cross-shore scale in the mid and upper water column.
3. Cross-shore asymmetry in the distribution of produced water occurs near the bottom where the produced water extends southward (across isobaths) from the diffuser.
4. Exposure to produced water will vary strongly with depth in spring–summer and vary weakly with depth in fall-winter.

While the existing biological observations are valuable, they cannot be used to test these predictions. The experiments of Raimondi and Schmitt (1992) were conducted only during periods of weak stratification and were of limited duration (a few hours to a few days). Those of Osenberg et al. (1992) were longer in duration, since they spanned summer-fall (June–October, 1990), but are unable to resolve temporal variations smaller than the experimental period. Experiments of Krause et al. (1992) and Krause (1993) also were of limited duration and did not resolve seasonal changes.

5. Conclusions

We conducted a combined field and modeling study to investigate the dispersion of produced water around a diffuser near Carpinteria, California. Observations of currents and water properties were used as inputs for a model of buoyant plume dispersal. The model simulated the dispersion and spatial distribution of produced water in the near-field around the diffuser. Far field dispersion was simulated using an elementary solution to the diffusion equation in combination with the current observations.

The observations show that strong thermal stratification prevails in spring and summer and weak stratification in fall and winter. No seasonal trend in currents is found. Currents at mid-depth flow along isobaths while those near the bottom frequently have an offshore, cross-isobath component. For 90% of the observations, currents speeds are 0.1 m s^{-1} or less.

A primary factor controlling the exposure of organisms to produced water around the diffuser is the depth range of the plume in the water column. The plume depth is modulated by seasonal changes in stratification. The plume is trapped below the surface in spring and summer and intermittently in winter due to freshening by winter storms. In fall and winter, it is mixed vertically through most of the water column.

Visitation frequency diagrams, constructed from current observations, indicate that produced water distributions exhibit east–west (along-isobath) symmetry in the mid-water column. This symmetry is in qualitative agreement with results from biological studies investigating the along-shore pattern of produced water impacts on various invertebrate species. Near the bottom the pattern of visitation frequency indicates that the produced water distributions are displaced offshore.

Initial dilution of produced water in the near-field depends on stratification and current speed. Minimum values of order 50–100 occur in summer with strong stratification and low current speed; maximum values of 500 occur in winter for low stratification and higher speeds (order 0.1 m s^{-1}). These represent the maximum concentrations to which organisms are generally exposed in the near field. Higher concentrations are possible in the initial mixing zone extending up to ~ 80 m from the diffuser.

Because of mixing processes and variable currents, dilution in the far-field is much higher than initial dilution. However, far-field dilutions are poorly constrained due to uncertainties in ambient mixing rates. We estimate that within 1000 m of the diffuser (along-shore), ambient mixing processes increase dilution by factors of order 10 to 10^3 when the plume is present in the far field. Because the plume is not always present at any given point, time-averaged dilutions are larger still by factors of 10^2–10^3. Our results support the conclusion of Krause (1993) that toxic effects are detectable at least 1000 m from the diffuser.

Acknowledgements

We thank Anne Petrenko and Brian Emery for helpful comments on an early draft of the manuscript. We also thank William Ford of Chevron, Inc. for providing detailed information about the diffuser and produced water discharge at the Carpinteria site. Krisada Lertchareonyong provided valuable assistance with programming. We thank Chris Gotshalk for help with field work. This research was funded by the UC Coastal Toxicology Program and by the Minerals Management Service, US Department of Interior under MMS Agreement No. 14-35-0001-3071. The view and conclusions in this paper are those of the authors and should not be interpreted as necessarily representing the official policies, either expressed or implied, of the US Government.

References

Baumgartner, D.J., Frick, W.E., Roberts, P.J.W., 1994. Dilution Models for Effluent Discharges, 3rd ed. US Environmental Protection Agency Report no. EPA/600/R-94/086, Washington, DC.

Fischer, H.B., List, E.J., Koh, R.C.Y., Imberger, J., Brooks, N.H., 1979. Mixing in Inland and Coastal Waters. Academic Press, New York.

Higashi, R.M., Cherr, G.N., Bergens, C.A., Fan, T.-W.M., 1992. An approach to toxicant isolation from a produced water source in the Santa Barbara Channel, In: Ray, J.P., Engelhardt, F.R., (Eds.), Produced Water: Technological/Environmental Issues and Solutions. Plenum Press, New York pp. 223–233.

Koh, C.Y., Brooks, N.H., 1975. Fluid mechanics of waste-water disposal in the ocean. Annual Reviews in Fluid Mechanics 7, 187–211.

Krause, P., 1993. Effects of poduced water on reproduction and early life stages of the purple sea urchin (*Strongylocentrotus Purpuratus*): field and laboratory tests. Ph.D. Dissertation, UCSB, 140 p.

Krause, P.R., Osenberg, C.W., Schmitt, R.J., 1992. Effects of produced water on early life stages of a sea urchin: stage-specific responses and delayed expression. In: Ray, J.P., Engelhardt, F.R., (Eds.), Produced Water: Technological/Environmental Issues and Solutions. Plenum Press, Newyork pp. 431–444.

Lee, R.S., Pritchard, T.R., 1996. Dispersion of effluent from Sydney's new deepwater outfalls, Part 1: Ocean processes, In: Pttiaratchi, C. (Ed.), Coastal and Estuarine Studies. American Geophysical Union, Washington, DC, 430–438.

List, E.J., 1982. Turbulent jets and plumes. Annual Reviews in Fluid. Mechanics 14, 189–212.

Okubo, A., 1980. Diffusion and Ecological Problems: Mathematical Models. Springer,Berlin 254p

Osenberg, C.W., Schmitt, R.J., Holbrook, S.J., Canestro, D., 1992. Spatial scale of ecological effects associated with an open coast discharge of produced water. In: Produced Water: Technological/Environmental Issues and Solutions. Plenum Press, New York, pp. 387–402.

Petrenko, A.A., Jones, B.H., Dickey, T.D., 1998. Shape and near-field dilution of the Sand Island sewage plume observations compared to model results. Journal of Hydraulic Engineering, 124, 565–571.

Pritchard, T.R., Lee, R.S., Davison, A., 1996. Dispersion of effluent from Sydney's new deepwater outfalls, Part 2: Observations of plume behaviour: winter and summer examples. In: Pttiaratchi, C. (Ed.), Coastal and Estuarine Studies. American Geophysical Union, Washington, DC, pp. 439–452.

Raimondi, P.T., Schmitt, R.J., 1992. Effects of Produced Water on Settlement of Larvae: Field Tests Using Red Abalone. In: Produced Water: Technological/Environmental Issues and Solutions. Plenum Press, New York, pp. 415–430.

Roberts, P.J.W., 1990. Outfall design considerations, In: Le Mehaute, B., Hanes, D.M. (Eds.), The Sea, Ocean Engineering Science. Wiley InterScience, New York.

Roberts, P.J.W., Snyder, W.H., Baumgartner, D.J., 1989a. Ocean outfalls. I: submerged wastefield formation, Journal of Hydraulic Engrineering 115, 1–25.

Roberts, P.J.W., Snyder, W.H., Baumgartner, D.J., 1989b. Ocean outfalls. II: spatial evolution of submerged wastefield. Journal of Hydraulic Engineering 115, 26–48.

Roberts, P.J.W., Snyder, W.H., Baumgartner, D.J., 1989c. Ocean outfalls. III: effect of diffuser design on the submerged wastefield. Journal of Hydraulic Engineering 115, 49–70.

Stephenson, M.T., 1992 A survey of produced water studies, In: Ray, J.P., Engelhardt, F.R. (Eds.), Produced Water: Technological/Environmental Issues and Solutions. Plenum Press, New York, pp. 1–11.

Stone, S., 1995. Spatial scale of produced water impacts as indicated by plume dynamics and biological field assays. Masters Thesis, University CA. Santa Barbara.

Washburn, L., Jones, B.H., Bratkovich, A., Dickey, T.D., Chen, M.S., 1992. Mixing, dispersion, and resuspension in the vicinity of an ocean wastewater plume. Journal of Hydraulic Engineering 118 (1), 38–58.

Winant, C.D., Olson, J.R., 1976. The vertical structure of coastal currents. Deep-Sea Research, 23, 925–936.

Wu, Y., 1993. The study of an ocean outfall buoyant plume near Whites Point, California. Ph.D. Dissertation, University of Southern California.

Wu, Y., Washburn, L., Jones, B.H., 1994. Buoyant plume dispersion in a coastal environment: Evolving plume structure and dynamics. Continental Shelf Research 14, 1001–1023.